An experimental and theoretical study of the gas-phase decomposition of monoprotonated peptide nucleic acids

ARTICLE *in* JOURNAL OF THE AMERICAN SOCIETY FOR MASS SPECTROMETRY · AUGUST 2000

Impact Factor: 2.95 · DOI: 10.1016/S1044-0305(00)00126-4 · Source: PubMed

An Experimental and Theoretical Study of the Gas-Phase Decomposition of Monoprotonated Peptide Nucleic Acids

Jason W. Flora, Donald D. Shillady, and David C. Muddiman
Department of Chemistry, Virginia Commonwealth University, Richmond, Virginia, USA

Peptide nucleic acids (PNAs) are DNA/RNA mimics which have recently generated considerable interest due to their potential use as antisense and antigene therapeutics and as diagnostic and molecular biology tools. These synthetic biomolecules were designed with improved properties over corresponding oligonucleotides such as greater binding affinity to complementary nucleic acids, enhanced cellular uptake, and greater stability in biological systems. Because of the stability and unique structure of PNAs, traditional sequence confirmation methods are not effective. Alternatively, electrospray ionization coupled with Fourier transform ion cyclotron resonance mass spectrometry shows great potential as a tool for the characterization and structural elucidation of these oligonucleotide analogs. Extensive gas-phase fragmentation studies of a mixed nucleobase 4-mer (AACT) and a mixed nucleobase 4-mer with an acetylated N-terminus (N-acetylated AACT) have been performed. Gas-phase collision-induced dissociation of PNAs resulted in water loss, cleavage of the methylene carbonyl linker containing a nucleobase, cleavage of the peptide bond, and the loss of nucleobases. These studies show that the fragmentation behavior of PNAs resembles that of both peptides and oligonucleotides. Molecular mechanics (MM+), semiempirical (AM1), and ab initio (STO-3G) calculations were used to investigate the site of protonation and determine potential low energy conformations. Computational methods were also employed to study prospective intramolecular interactions and provide insight into potential fragmentation mechanisms. (J Am Soc Mass Spectrom 2000, 11, 615–625) © 2000 American Society for Mass Spectrometry

Recently there has been a serious effort by the medical and biochemical communities in the design, synthesis, and investigation of various synthetic DNA and RNA mimics. The modifications of the oligonucleotide structure include alteration of the phosphate group, the deoxyribose sugar, and the attached nucleobases [1]. The variety of structural enhancements are intended to not only improve the oligonucleotide derivatives' binding ability to targeted nucleic acid receptors but also lend to their resistance to enzymatic degradation and increase their cell membrane permeability [2].

Peptide or polyamide nucleic acids (PNAs), Figure 1, [3–6] are DNA/RNA mimics which have recently generated considerable interest due to their potential use as antisense and antigene therapeutics (translation and transcription inhibitors, respectively) and as diagnostic and molecular biology tools [7, 8]. These molecules are achiral and neutral oligonucleotide analogs consisting of nucleobases linked to a repeating N-(2-aminoethyl) glycine backbone which is homomorphous with the DNA phosphate backbone [4]. PNAs were designed with optimal spacing between nucleobases and a neutral backbone in order for them to bind to complementary DNA and RNA strands with higher affinity and specificity than oligonucleotides [4, 9, 10]. PNAs are known to bind to complementary DNA strands by Waston–Crick and in some cases Hoogsteen base pairing [11]. PNAs have also demonstrated extraordinarily high biostability in cell extracts and human serum [12]. The unique structure of PNAs makes them resistant to degradation by enzymes such as nucleases and proteases because they do not easily recognize the polyamide backbone and nucleobase side chains.

Because of the structure of PNAs, traditional sequencing techniques are ineffective [13–16]. An alternative method for the structural elucidation of these important DNA/RNA mimics is the use of mass spectrometry (MS). Previous studies have demonstrated that electrospray ionization (ESI) is a versatile method for ionizing peptides, proteins, and oligonucleotides [17–19]. Peptide and protein cations and oligonucleotide anions have been subjected to tandem mass spectrometry which has repeatedly resulted in structurally informative cleavages with dominant, competitive, and consecutive reaction fragmentation pathways [20–23].

Address reprint requests to Dr. David C. Muddiman, Virginia Commonwealth University, Department of Chemistry, 1001 West Main Street, Richmond, Virginia 23284. E-mail: dcmuddim@saturn.vcu.edu

1044-0305/00/$20.00
PII S1044-0305(00)00126-4

Received December 15, 1999
Revised March 9, 2000
Accepted March 9, 2000

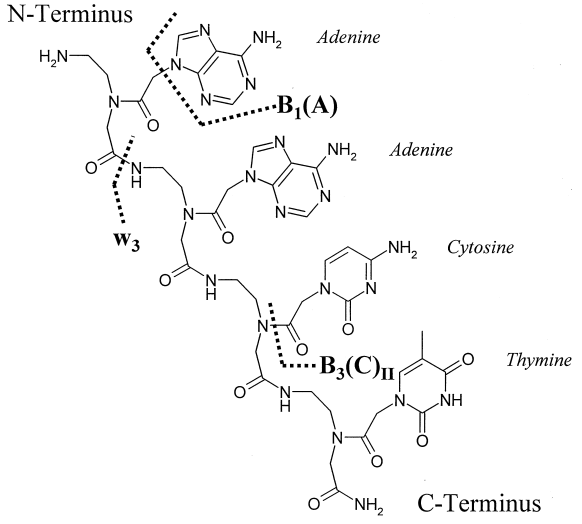

Figure 1. The nomenclature designations for fragmentations observed for the mixed nucleobase 4-mer PNA AACT [30]. The PNA backbone cleavage of the peptide bond, w_3, corresponds to the peptide backbone cleavage, Y_n [79]. The $B_n(A)$ cleavage is the loss of an adenine. The cleavage of a nucleobase involves the ionizing proton residing on the leaving nucleobase; this results in a neutral nucleobase loss. $B_3(C)_{II}$ is the cleavage of the methylene carbonyl linker containing the nucleobase cytosine. A cleavage of a methylene carbonyl linker containing a nucleobase involves a proton transfer from the departing fragment to the main product ion.

Studies of these gas-phase biomolecules have shown that one or more stages of collision-induced dissociation (CID) could potentially provide complete sequence information [21, 24–26]. Therefore, tandem ESI-MS should potentially provide data for sufficient characterization and structural elucidation of these oligonucleotide derivatives, PNAs, and their degradation products [27–30].

The information obtained from modern computational chemistry is commonly being used to interpret and supplement various forms of experimental chemical data. The use of computational chemistry for gas-phase studies on peptide cations and oligonucleotide anions has provided valuable information on their inherent behavior in the gas phase. These theoretical calculations can also help predict the site of protonation, which is significant because it is generally accepted that the position at which a charge resides often directs the dissociation pathways of biomolecules [31–37]. Computational studies have been conducted that provided information on intramolecular hydrogen bonding and its effects on molecular structure and stability [31, 38] as well as determining proton affinities (PA) of some amino acids and peptides (i.e., of polyglycines) [32, 39–42]. Recent protonation studies have shown that intramolecular interactions such as hydrogen bonding significantly increases gas-phase basicity (GB) and PA of amino acids [38, 43–49]. As mentioned before, PNAs have a neutral modified polyglycine backbone which is a strong indication that the backbone proton affinities and intramolecular interactions will be comparable to that of polyglycines and other related peptides. PNAs also contain nucleobases attached to the peptide-like backbone by a methylene carbonyl linker; therefore, some analogous oligonucleotide gas-phase behavior is also predicted (i.e., nucleobase loss).

An understanding of the relative proton affinity of the various basic sites, the initial site of protonation, and potential intramolecular interactions, obtainable by computational chemistry, can provide invaluable information when determining gas-phase decomposition mechanisms. This paper reports our findings from an experimental and theoretical investigation of the gas-phase fragmentation pathways of monoprotonated PNAs in an effort to determine fragmentation chemistry and develop methods for the structural elucidation of these oligonucleotide analogs. We will also present peptide nucleic acid decomposition mechanisms supported by the theoretical calculations performed with the molecular mechanics force field MM+, the semiempirical method AM1, and the ab initio basis set STO-3G. In these investigations, monoprotonated PNAs were produced by ESI in conjunction with Fourier transform ion cyclotron resonance mass spectrometry (FTICR-MS). The CID methods employed were sustained off-resonance irradiation (SORI) [50] and nozzle–skimmer (NS) [51–53] dissociation.

Experimental

Materials

The peptide nucleic acids used in this study (AACT and N-acetylated AACT) were custom synthesized and purified (HPLC) by Commonwealth Biotechnologies (Richmond, VA). The PNA synthesis utilized the 9-fluorenylmethyloxycarbonyl (Fmoc) protecting group strategy where the resulting PNAs were obtained as their C-terminal amides [54]. The acetonitrile, ammonium acetate, and acetic acid were purchased from Sigma-Aldrich (St. Louis, MO). All the materials were used as received and all solvents were spectra grade.

Mass Spectrometry

All experiments were conducted on microspray sources equipped with ESI emitters that were hand-pulled over a Bunsen burner from 50 μm i.d., 181 μm o.d., fused-silica capillaries (Polymicro Technologies, Phoenix, AZ) creating a taper of 50 to 10 μm [55]. PNA electrospray solutions consisted of 1:1 acetonitrile: 10 mM ammonium acetate (v/v) with the addition of 0.5% to 1.0% acetic acid (v/v). Infusion was performed using a Harvard Syringe pump, model PHD 2000 Infusion, at a rate of 250 nL/min, through a 20 μL Hamilton syringe held at a potential of ~2 keV.

A modified Ionspec Corporation (Irvine, CA) FTICR-MS was used for all experiments and data collection. All data processing and signal generation were

Table 1.

Experimental mass, Da	Mass loss, Da	Relative intensity, %	Assigned fragment	Theoretical mass, Da	Relative mass error, ppm	Molecular formula
1085.45	—	100	$[M + H]^+$	1085.46	−9.21	$C_{43}H_{57}N_{24}O_{11}$
MS^2 of m/z = 1085.5 (nozzle–skimmer)						
1067.44	18.01	100	$[M + H - \mathbf{H_2O}]^+$	1067.45	−9.37	$C_{43}H_{55}N_{24}O_{10}$
MS^3 of m/z = 1067.4 (SORI applied at m/z = 1083.6); KE_{lab} = 4.3 eV						
932.37	135.03	13.93	$[M + H - H_2O - \mathbf{B_n(A)}]^+$	932.40	−32.18	$C_{38}H_{50}N_{19}O_{10}$
916.38	151.02	32.17	$[M + H - H_2O - \mathbf{B_3(C)_{II}}]^+$	916.42	−43.65	$C_{37}H_{50}N_{21}O_8$
810.33	257.07	12.76	$[\mathbf{w'_3} + H]^+$	810.35	−24.68	$C_{32}H_{44}N_{17}O_9$
792.32	275.08	32.91	$[\mathbf{w'_3} + H - H_2O]^+$	792.34	−25.24	$C_{32}H_{42}N_{17}O_8$
781.34	286.06	4.85	$[M + H - H_2O - \mathbf{B_3(C)_{II} - B_n(A)}]^+$	781.36	−25.60	$C_{32}H_{45}N_{16}O_8$
1049.41	18.00	3.37	$[M + H - \mathbf{2}H_2O]^+$	1049.44	−28.59	$C_{43}H_{54}N_{24}O_9$
MS^4 of m/z = 932.4 (SORI applied at m/z = 944.7); KE_{lab} = 4.9 eV						
781.33	151.03	100	$[M + H - H_2O - \mathbf{B_3(C)_{II} - B_n(A)}]^+$	781.36	−38.39	$C_{32}H_{45}N_{16}O_8$
MS^4 of m/z = 916.4 (SORI applied at m/z = 928.3); KE_{lab} = 5.0 eV						
641.28	275.10	100	$[\mathbf{w'_3} + H - H_2O - B_3(C)_{II}]^+$	641.30	−31.19	$C_{26}H_{37}N_{14}O_6$
MS^4 of m/z = 810.3 (SORI applied at m/z = 819.6); KE_{lab} = 5.7 eV						
792.31	18.01	100	$[w'_3 + H - H_2O]^+$	792.34	−37.86	$C_{32}H_{42}N_{17}O_8$
MS^4 of m/z = 792.3 (SORI applied at m/z = 801.2); KE_{lab} = 5.8 eV						
641.29	151.03	100	$[w'_3 + H - H_2O - \mathbf{B_3(C)_{II}}]^+$	641.30	−15.59	$C_{26}H_{37}N_{14}O_6$

conducted on an Ionspec Omega 586 data station. The analog-to-digital converter digitizes signals to 10 bits of precision at a sampling rate of 1 MHz. This instrument is equipped with a 4.7 tesla horizontal bore superconducting magnet with a 128 mm bore (Cryomagnetics, Oak Ridge, TN). Over a 2 in. diameter and 4 in. in the axial direction the magnet's central field homogeneity is ±0.001%. The mass spectrometer's high-speed shutter was connected to a Keithly 617 Programmable Electrometer (picoammeter) used to indicate the stability of the electrospray ionization (~20 pA) [55, 56].

Ion trapping was performed in the axial direction by applying an asymmetric trapping well with 9 V applied to the front trapping plate and 10 V to the back trapping plate. The trapping was improved by introducing molecular nitrogen trapping gas at a pressure of approximately 1×10^{-5} torr. Ion excitation covered an m/z range of 200 to 2500 in 4 ms using a Chirp waveform with an excitation amplitude of 40 $V_{p\text{-}p}$. This broadband frequency-sweep excitation results in a maximum ion radius of approximately 0.684 cm, assuming a dipolar geometry factor ($\beta_{dipolar}$) of 0.72167 and the distance between excitation plates is 5 cm [57].

An arbitrary waveform generator was used to perform ion isolation by ejecting all ions from the ICR cell that have higher or lower frequencies than the ion of interest by the application of excitation pulses with an amplitude that increases the cyclotron radius to where it exceeds the physical boundaries of the cell. The FTICR-MS was externally calibrated using the +10, +11, and +12 charge states of bovine ubiquitin. The mass accuracy of the calibration was then tested using bovine insulin and resulted in an error of less than 10 ppm.

Two CID methods were employed during our investigation of PNAs, SORI [50], and nozzle–skimmer [51–53]. Both CID events result in multiple low-energy collisions that can activate the ion until it dissociates [50]. The SORI method involved a 2 s rf excitation with the optimal amplitude of 6.0 $V_{p\text{-}p}$, at a frequency 1000 Hz lower than the precursor ion and in the presence of molecular nitrogen as the collision target. All average kinetic energy in laboratory system of coordinates (KE_{lab}) are reported for each SORI dissociation event in Table 1. The nozzle skimmer (in-source CID) potential difference was 215 V for all experiments that utilized this CID method.

Theoretical Calculations

Molecular mechanics and semiempirical calculation were performed on a Pentium II 450 MHz PC with 384 MBytes of RAM and equipped with the computational software package Hyperchem 5.1 with the ChemPlus Modules. Each PNA studied had a Monte Carlo conformational search, a feature of the ChemPlus Modules, of the neutral structure using the MM+ force field, an extension of MM2 [58], in order to find a potentially global minimum configuration. These searches were loose optimizations using random walks and rotating all single bonds. The range for acyclic torsion variation was set at ±60 to 180, avoiding eclipsed orientations, and the range for ring torsion flexing was set at ±30 to 120. The searches were terminated after 100,000 iterations or 300 optimizations keeping no more than 50 configurations that were less than 6 kcal/mol above the best configuration.

After minimized structures are determined by a conformational search, the semiempirical method employed for all geometry optimizations and proton affin-

ity calculations of the modified and unmodified 4-mer PNAs was the AM1 theoretical model [40, 59]. Geometry optimizations using the quantum method AM1 were performed on the five lowest energy configurations resulting from the initial molecular mechanics conformation search. This allowed verification or necessary adjustments to the ordering, starting with the lowest energy structure, of closely related energy levels. Because molecular mechanics is an entirely different approach to the treatment of molecular geometry than quantum methods, there are often slight changes in the ordering of closely related configurations. In some cases the ordering was changed when the PNAs were optimized by AM1. In all cases the lowest energy configuration resulting from the quantum optimization was used for all proton affinity calculations and geometry interpretation (i.e., intramolecular interactions).

The theoretical model AM1 is an improvement over MNDO especially for compounds containing nitrogen and oxygen and considered to be one of the most accurate semiempirical methods [59]. The AM1 model is useful for organic molecules that contain elements from the first and second rows of the periodic table. This semiempirical method is also known to repeatedly demonstrate accurate reproduction of experimental trends [40]. It has been demonstrated that when using the AM1 method a reasonable correlation between experimental and theoretical results occurs when comparing structurally similar compounds [40, 60]. However, AM1 does tend to underestimate proton affinities of amines, but, not as severely as MNDO [40]. Therefore, because PA values calculated by AM1 are best used to compare trends within similar groups of compounds, no absolute values will be reported. Trends in PA and minimized structures were the goal of this computational investigation and furthermore, reported PA values should be produced by experimental means accompanied by computational data.

Ab initio calculation were performed on 1-mer PNA units to provide verification of semiempirical trends. The GAMESS software with the STO-3G basis set was used for these calculations [61–63]. These calculations were carried out on a silicon graphics Origin 2000 using only one processor (250 MHz R10000, 64 bit CPU). Proton affinities were calculated by optimizing the energy minimum after placing a proton at the desired location. A convergence limit was set at 0.001 au for a maximum of 200 iterations. Even with preoptimized neutral species as starting geometries, up to 180 iterations were required to reach the 0.001 au gradient. The ab initio calculations cannot be applied to larger PNA sequences due to the size limitations of high level calculations; therefore, semiempirical values provide PA trend information for all structures larger than 1-mers.

Results and Discussion

Computational Investigation of Monoprotonated Peptide Nucleic Acids

The ionization methods employed for mass spectrometry often involve cation coordination. The experiments discussed in this paper all involve monoprotonated PNA oligomers generated by ESI. Because many low energy CID fragmentation mechanisms are charge directed [33, 34, 64–68], the determination of the site of protonation, intrinsic proton affinities, and potential intramolecular hydrogen bond interactions can provide important information regarding gas-phase molecular ion decomposition. Subsequently, we employed computational chemistry during our investigation of monoprotonated PNAs in order to provide further insight into the interpretation and understanding of the CID of this unique biomolecule. The results of this computational investigation will be reported first in order to provide some background and support of the interpretation of the following experimental data.

Determination of the initial site of protonation of peptide nucleic acids. There have been multiple studies on the site of protonation of neutral peptide oligomers [38, 39, 44, 46, 48, 60, 69–72]. Each of these studies (e.g., polyglycines) agree that the site of protonation for neutral polypeptides is the N-terminus [32, 38, 39, 44, 46, 48, 60, 69–75]. In addition, high level ab initio calculations by Zhang and co-workers demonstrate with a large degree of certainty that the preferred site of protonation of polyglycines is indeed the terminal amino nitrogen [39].

Proton affinities of all PNA 4-mer basic sites (all nitrogens and oxygens) were calculated using the data from semiempirical geometry optimizations. It is important to note that the N-terminus of the modified polyglycine PNA backbone is a primary amine attached to two consecutive carbons. This ethyl linker increases the base strength of the amine by releasing electrons to the nitrogen. When the primary amine is protonated, the positive charge is more effectively dispersed by the attached alkyl group resulting in greater ion stability. Subsequently, according to our semiempirical calculations and analogous to all nonbasic peptides (peptides without lysine, histidine, and arginine) the most basic site on PNA oligomers is the N-terminus [32, 39, 42, 73–75]. The proton affinity value of the N-terminus calculated for the PNA AACT potential minimized geometry is 237.1 kcal/mol, which based upon the results recently demonstrated by Limbach and co-workers [76, 77] would suggest competition for the proton between the attached nucleobases and the N-terminus. However, the PNA proton affinities were calculated by AM1, a semiempirical method which is known for underestimating PA values for amines [40]. According to our PA calculations of all basic sites on the potential

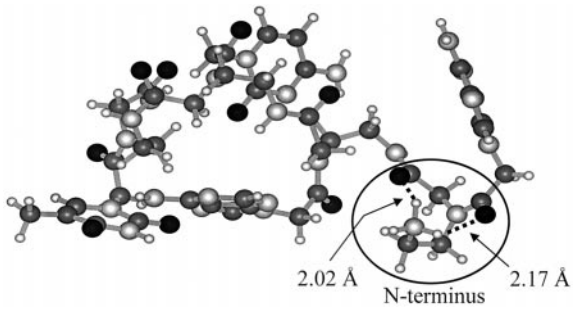

Figure 2. Minimized structure of PNA AACT resulting from a conformational search (MM+) and geometry optimization (AM1). Intramolecular interactions between a hydrogen on the protonated N-terminus and the carbonyl oxygen on the backbone closest to the N-terminus and between a hydrogen on the protonated N-terminus and the carbonyl oxygen on the methylene carbonyl linker closest to the N-terminus. The intramolecular hydrogen bond lengths are 2.02 and 2.17 Å, respectively. Oxygens are black; nitrogens are light grey (big); carbons are dark grey; and hydrogens are light grey (small).

minimum conformations of AACT, protonation of the N-terminus was energetically favored.

Ab initio calculations were performed on 1-mer PNA units using STO-3G to verify trends observed for the semiempirical calculations performed on the 4-mer PNA units. Because of size limitations, ab initio calculations could not be carried out on PNA units larger than 1-mers, which are on average about 37 atoms. These higher level calculations showed the same trends in the proton affinity as observed at the semiempirical level for the PNA AACT. For the potential minimum geometries of the 1-mers containing adenine, guanine, cytosine, and thymine the most basic site is clearly the primary amine on the N-terminus. Again, suggesting that the N-terminus is the preferred site of protonation and subsequently the initial site where the charging proton resides.

Potential intramolecular interactions. Intramolecular interactions have been known to greatly increase the proton affinity of amino acids [32, 38, 39, 60, 70, 72–75, 78]. In peptide configurations, hydrogen bonding between a protonated terminal amine and neighboring carbonyl oxygens increases molecular stabilization and thus increases the proton affinity [32, 38, 39, 60, 70, 73–75, 78]. Hydrogen bonding is typically characterized by distances between the hydrogen and the interacting atom (e.g., carbonyl oxygen) of less than 2.6 Å [38]. Zhang et al., using ab initio calculations, and Lebrilla and Wu, using AM1 calculations, demonstrated that the lowest energy conformation for polyglycines involved protonation of the N-terminus and hydrogen bonding interactions between the N-terminus and the neighboring carbonyl oxygens [39, 60].

Figure 2 shows a potential global minimum geometry of the 4-mer AACT, $[M + H]^+$, resulting from a conformational search using MM+ and a geometry optimization using AM1. This conformation suggests that the potential PNA lowest energy structures experience hydrogen bonding at the N-terminus. The results of the calculations for AACT hydrogen bonds, displayed in Figure 2, show that the C=O···H–N bond length for a hydrogen on the protonated N-terminus and the carbonyl oxygen on the methylene carbonyl linker is 2.17 Å and for a hydrogen on the protonated N-terminus and the carbonyl oxygen on the backbone is 2.02 Å. According to our semiempirical calculations performed on this potential minimum energy structure, the PA of the carbonyl oxygen on the backbone, Figure 2, is ~15 kcal/mol greater than the carbonyl oxygen on the methylene carbonyl linker. Intuitively, this difference in PA corresponds to the difference in hydrogen bond lengths.

Multistage-Mass Spectrometric Analysis of Fragment Ions Produced by Collisional Activation of Monoprotonated Peptide Nucleic Acids

Peptide nucleic acid fragmentation nomenclature. Prior to our investigations of PNAs, no comprehensive nomenclature that could account for all possible PNA cleavage sites existed. Subsequently, we developed a descriptive nomenclature that could describe all potential PNA fragment ions [30]. It is important to note that PNAs are basically a hybrid of both peptides and oligonucleotides; therefore, our PNA nomenclature is inherently a hybrid of both the widely accepted peptide [23, 79] and oligonucleotide [20, 21] nomenclatures. For the readers convenience, Figure 1 (AACT) shows the fragment ions that we observed during our investigation of the monoprotonated PNA 4-mers. In summary, w_3' ions refer to cleavage of the PNA peptide bond closest to the N-terminus. The prime refers to a hydrogen atom that has been transferred from the departing fragment to the product ion [20, 79]. The neutral loss of the first nucleobase, adenine, is designated as $-B_1(A)$. The subscript, one, signifies that it is the first nucleobase starting from the N-terminus. The neutral loss of the nucleobase cytosine attached to the methylene carbonyl linker is referred to as $-B_3(C)_{II}$. The subscripts 3 and II designate that it is the third nucleobase from the N-terminus and the cleavage occurred at the amide bond on the methylene carbonyl linker, respectively, see Figure 1. The origin of these cleavage mechanisms will be discussed in detail later and this nomenclature will be used throughout this paper.

Tandem-mass spectrometry of the 4-mer PNA AACT $[M + H]^+$ ion. Table 1 summarizes the data for all four stages of mass spectrometry for the PNA AACT. All mass losses are reported from experimental monoisotopic peaks and relative intensities are calculated from peak amplitudes (magnitude mode). The fragment assignments, using the PNA nomenclature [30], are made from the calculated mass losses. It is important to note that high-mass accuracy was obtained for all PNAs

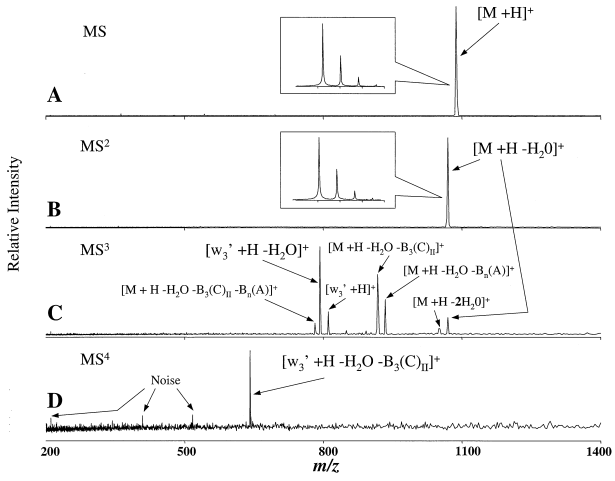

Figure 3. Four stages of mass spectrometry obtained for one of the observed fragmentation pathways of the mixed nucleobase 4-mer PNA AACT. (**A**) +1 charge state of the intact PNA providing low ppm mass accuracy. (**B**) Nozzle–skimmer dissociation potential difference of 215 V for the molecular ion shown in 2A which resulted in only loss of water. (**C**) Ion isolation of m/z = 1067.4; SORI-CID applied at m/z = 1083.6 (1000 Hz off-resonance) with an amplitude of 6.0 $V_{p\text{-}p}$ resulting in a KE_{lab} = 4.3 eV. (**D**) Ion isolation of m/z = 792.3; SORI-CID applied at m/z = 801.2 (1000 Hz off-resonance) with an amplitude of 6.0 $V_{p\text{-}p}$ resulting in a KE_{lab} = 5.8 eV.

investigated and ranged from ±45 ppm (0.045 in 1000 Da). All mechanisms proposed in this section are derived from, and consistent with, experimental and theoretical data. As with many proposed mechanism, these have not been thoroughly validated; however, they provide a solid basis from which future studies can be based.

Figure 3 shows four stages of mass spectrometry for the PNA AACT. Figure 3A is the spectra of the ion isolation of the intact isotopic envelope of the $[M + H]^+$ ion. Figure 3B shows the second stage of mass spectrometry where the only mass loss observed is 18.01 Da. This product ion corresponds to the loss of water and is designated as $[M + H - H_2O]^+$. SORI (6.0 $V_{p\text{-}p}$) and nozzle–skimmer dissociation (NS at 215 V) of the precursor ions of AACT result in only the initial loss of water. It has been previously shown that peptides experience some water loss but not dominantly as with PNAs [80]. Therefore, the regularity at which water loss appears can be attributed to a structural difference between PNAs and peptides. The structural variation that is most suspicious of generating a high abundance of water loss is the PNA's modified C-terminus. Because of an artifact of the Fmoc protecting group synthesis which results in increased water solubility and the prevention of self aggregation [81], PNAs do not have a true C-terminus. The C-terminus of the PNAs used in this research (see Figure 1) is not a traditional carboxyl group but a primary amide. Fortuitously, the gas-phase thermal decomposition of amides and polyamides has been extensively studied [82]. Thermal decomposition of primary amides resulting in

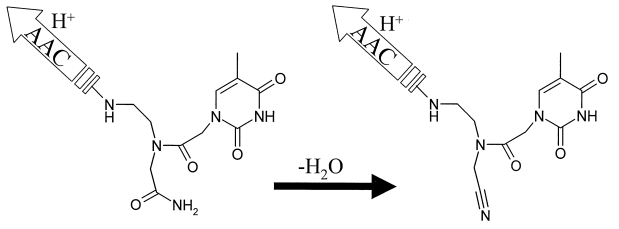

Scheme 1.

the formation of nitriles have been previously demonstrated using infrared spectroscopy, gas chromatography Fourier transform infrared spectroscopy, and gas chromatography mass spectrometry [82]. Scheme **1** shows a proposed mechanism for the dehydration of the PNA C-terminus analogous to the gas-phase thermal decomposition mechanisms previously proposed [82]. When the precursor ion is subjected to CID, sufficient internal energy can result in promoting rearrangement of the C-terminus and subsequent loss of H_2O, leaving a nitrile at the C-terminus. It is important to note that this water-loss mechanism is charge remote, independent of the location of the proton.

Because of a product ion in the third stage of mass spectrometry $[w_3' + H]^+$, which will be discussed in detail later, and the existence of fragment ions that have lost two water molecules, the above water loss mechanism (Scheme **1**) cannot account for all of the dehydration of PNA ions. There have been several mechanisms proposed for the peptide water loss involving the carboxyl C-terminus or the various amide oxygens along the peptide backbone. Because PNAs do not have a true C-terminus or acidic residue the only previously proposed peptide mechanism that can apply involves the amide oxygens and is referred to as the retro-Ritter reaction [80, 83]. This reaction suggests that a triple bond results across the peptide bond creating a nitrillium ion [80, 83]. However, this bond, the suggested C≡N triple bond, would have to cleave in the third stage of mass spectrometry, to account for observed product ion, $[w_3' + H]^+$. This strongly suggests that the retro-Ritter reaction does not apply to the second water loss mechanism of PNAs; cleavage of a triple bond is unlikely.

The computational results for the 4-mer PNAs, discussed earlier and shown in Figure 2, suggest that there is potentially a large degree of hydrogen bonding between hydrogens on the protonated N-terminus and the neighboring carbonyl oxygen on the backbone and the carbonyl oxygen on the methylene carbonyl linker. Because of these interactions, under collisional activation conditions there is a high probability of proton migration from the N-terminus to these adjacent carbonyl oxygens. If the proton migrates to the carbonyl oxygen on the methylene carbonyl linker adjacent to the N-terminus, Scheme **2**, the carbonyl carbon essentially becomes even more electron deficient. Subsequently, the energy of activation of a nucleophilic attack from

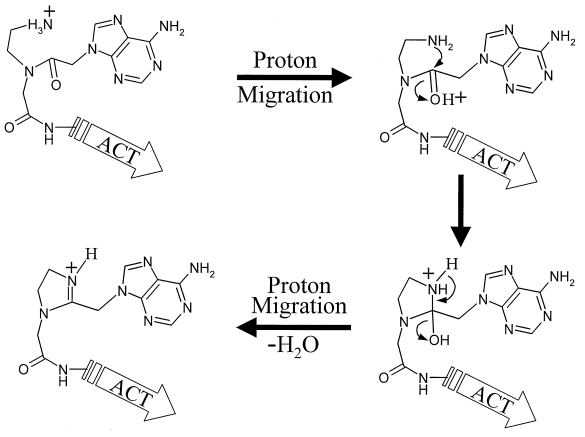

Scheme 2.

the electron rich primary amine on this carbonyl carbon is significantly decreased. A heterocyclic five-member ring forms, proton migration and dehydration occurs, and a mobile proton is released upon ring stabilization.

In the third stage of mass spectrometry, following PNA dehydration, the most abundant product ion, loss of 275.08 Da, corresponds to the cleavage of the PNA's peptide bond closest to the N-terminus where the initial site of water loss resides on the product ion, $[w_3' + H - H_2O]^+$ (Figure 3C). There has been previously proposed mechanisms for the cleavage of the peptide bond on protonated peptides that did not contain strongly basic residues [32, 68, 84–86]. We argue that a gas-phase mechanism analogous to that presented by Nold et al. is occurring for the PNA peptide bond cleavage [84].

Scheme **3** shows the steps involved in the formation of this w_3' ion [86]. As mentioned before, there is potentially a high degree of intramolecular interaction between the initially protonated N-terminus and the neighboring carbonyl oxygens. It is therefore likely that proton migration could occur to the carbonyl oxygen on the backbone. This peptide bond cleavage is initiated by proton migration to the amide nitrogen involved in the peptide bond which creates elongation of the C(=O)–N

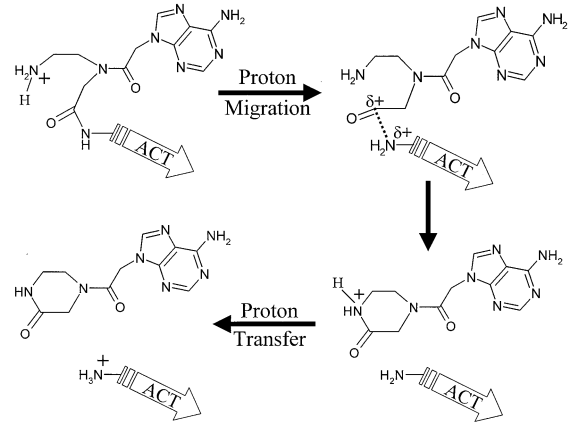

Scheme 3.

bond. It is known that for amides there are nonbonding and pi ($n-\pi$) conjugations of the nitrogen's lone pair of electrons and the adjacent carbonyl that add to the strength of the amide bond. It has been proposed and demonstrated, through ab initio and semiempirical calculations, that protonation of the amide nitrogen terminates this conjugation, thus appreciably weakening this bond [32, 87–89]. Extensive theoretical studies on peptides have concluded that the carbonyl oxygen participating in an amide bond is more energetically favorable for protonation than the amide nitrogen; however, there is a low energy barrier for protonation of the amide nitrogen [38, 39, 41, 60, 87]. In order for cleavage of the peptide bond to transpire, there must be an intramolecular proton transfer to the amide nitrogen [87].

Our molecular mechanics and semiempirical calculations on the C(=O)–N bond length show bond elongation of approximately 0.13 Å when the charging proton resides on the nitrogen of the amide bond. This bond length, a result of the terminated conjugation of the amide bond, causes further electron deficiency at the carbonyl carbon involved in the peptide bond. This carbon subsequently becomes more susceptible to nucleophilic attack by the N-terminal amine thus forming a six-membered ring, Scheme **3**. Upon ring formation a mobile proton is generated and the peptide bond cleaves. Competition for the mobile proton favors the more basic, newly formed, N-terminus over the carbonyl oxygen resulting in a neutral six-membered ring leaving group and a protonated C-terminal product ion, $[w_3' + H - H_2O]^+$. Cleavage of the peptide bond does not occur at any other locations on the PNA, thus supporting our belief that this mechanism involves the N-terminus.

Cleavage of the peptide bond is also observed in the third stage of mass spectrometry at low intensity (see Table 1) for product ions that lost water by way of the five-membered ring formation shown in Scheme **2**, loss of 257.07 Da. For these ions, $[w_3' + H]^+$ (Figure 3C), the 3-mer fragment ions do not posses a site of initial water loss suggesting that the C-terminus is still intact. A second mechanism for the cleavage of the peptide bond needs to be proposed because the mechanism of dehydration, in this case, is the formation of a ring involving the N-terminus and the neighboring methylene carbonyl linker. Scheme **2** demonstrates that the ring formation generates a mobile proton for this water loss mechanism. During collisional activation this proton can migrate to the nitrogen involved in the peptide bond closest to the N-terminus, Scheme **4**, bond elongation again results, significantly weakening the peptide bond [32]. The reaction proceeds comparable to protonated amide cleavage shown by Tu et al. for low collision energy [87]. An acylium ion/3-mer complex forms and the reaction proceeds via a ketene/3-mer complex bound by a proton (not shown) [87]. The charge is captured by the primary amine on the 3-mer because it undoubtedly has a greater proton affinity

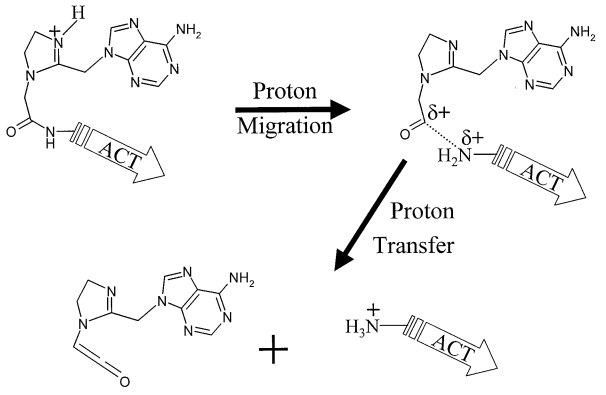

Scheme 4.

than the ketene. This cleavage is further supported by MS^4 data and will be discussed vida infra.

The second most abundant MS^3 product ion results from the loss of 151.02 Da. This fragment corresponds to the cleavage of the methylene carbonyl linker containing the cytosine with a hydrogen transfer from the leaving fragment to the main product ion; the product ion is designated as $[M + H - H_2O - B_3(C)_{II}]^+$. This mechanism, Scheme **5**, can be explained by proton migration to the tertiary amide that connects the methylene carbonyl linker of the cytosine to the PNA backbone. It is not clear why the proton migrates to the methylene carbonyl linker of the cytosine specifically. It has been previously reported from an investigation of a wide variety of PNA sequences that when several different bases are present in a sequence, the CID product ions corresponding to each base do not correlate with the frequency of occurrence of each base [90]. Base dependence to fragmentation pathway is not yet understood and will require more systematic studies of a large variety of PNAs. However, it is not surprising that when the charging proton breaks free from the N-terminus it chooses a tertiary amide. Extensive investigation of GB and PA of aliphatic carboxyamides clearly demonstrates that tertiary amides are more basic

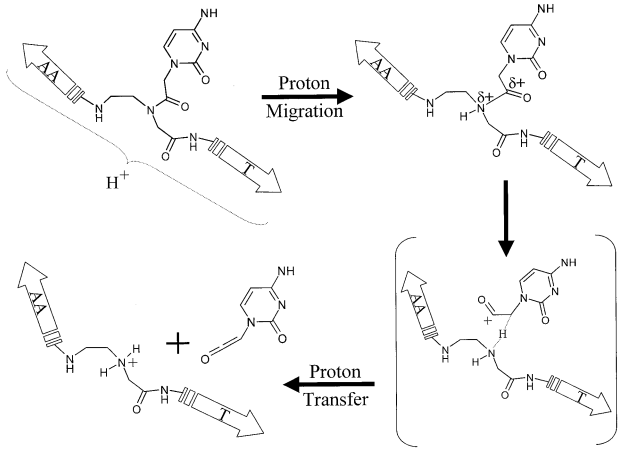

Scheme 5.

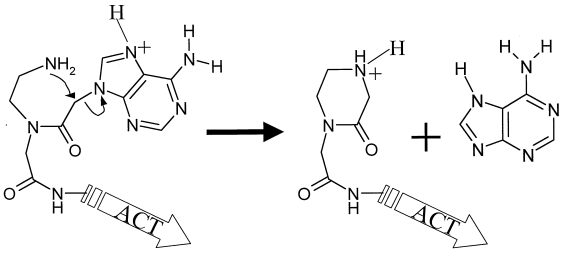

Scheme 6.

than secondary amides, which are more basic than primary amides [91]. It has also been previously discussed that protonation of the amide nitrogen causes significant weakening of the amide bond [32]. Computational methods again show that protonation of this nitrogen leads to bond lengthening of approximately 0.13 Å. Collisional activation induces bond cleavage at this weakened bond and an acylium ion/$[M - H_2O - B_3(C)_{II}]$ complex forms. This cleavage is also analogous to the low energy dissociation observed for protonated amides [87]. The resulting products are a neutral ketene and a protonated secondary amine [87]. The secondary amine has a higher proton affinity than that of the resulting ketene; therefore, the $[M + H - H_2O - B_3(C)_{II}]^+$ ion contains the mobile proton. Acylium ions were not detected in these experiments; however, these ions were observed, at low intensity because neutral ketene loss was favored, in later experiments involving a 6-mer cytosine homo-oligomer PNA (data not shown).

Analogous to oligonucleotide fragmentation, PNA nucleobases often cleave directly from the linkers as a result of collisional activation. The third most abundant MS^3 fragmentation is the loss of 135.03 Da. This mass loss correlates to the cleavage of the nucleobase adenine where the charging proton resides on the leaving nucleobase; the product ion is designated as $[M + H - H_2O - B_n(A)]^+$. It is important to note that semiempirical data suggests that for the 4-mer PNA AACT the adenine closest to the N-terminus is the second most basic site on the molecule. Furthermore, when a proton resides on the nucleobase adenine it becomes a good leaving group. The proposed mechanism for this base loss, Scheme **6**, involves a proton residing on the adenine. This proton, presumably on nitrogen 7, polarizes the bond attaching the nucleobase to the methylene carbonyl linker. Collisional activation induces cleavage of this bond resulting in the formation of a carbocation. The mechanism proceeds by stabilization of the carbocation by a nucleophilic attack of the terminal amine resulting in the formation of a heterocyclic six-member ring, which generates a mobile proton. This mechanism implies that single base loss only occurs by the nucleobase closest to the N-terminus.

The fifth most abundant product ion produced by MS^3 of AACT is the loss of 286.06 Da which corresponds to the cleavages of both the methylene carbonyl

linker containing the cytosine and the loss of the nucleobase adenine, designated as $[M + H - H_2O - B_3(C)_{II} - B_n(A)]^+$. Both cleavages require the presence of a mobile proton suggesting that these cleavages do not occur simultaneously.

Four stages of mass spectrometry were attempted on all fragment ions; however, for AACT only four of the six third stage product ions resulted in detectable ions (Table 1). SORI-CID of the product ion that resulted from the loss of the nucleobase adenine in the third stage of mass spectrometry, mass 932.36 Da and designated as $[M + H - H_2O - B_n(A)]^+$, resulted in the mass loss of 151.03 Da which corresponds to a cleavage of the methylene carbonyl linker containing the cytosine, $B_3(C)_{II}$, resulting in the product ion $[M + H - H_2O - B_n(A) - B_3(C)_{II}]^+$. Fragmentation of $[M + H - H_2O - B_3(C)_{II}]^+$ resulted in a loss of 275.10 Da which correlates to a cleavage of the peptide bond closest to the N-terminus where the MS^4 product ion is designated as $[w_3' + H - H_2O - B_3(C)_{II}]^+$. Collisional activation of the $[w_3' + H]^+$ ion, the product ion that does not contain the site of initial water loss at the C-terminus, loses only 18.01 Da, the mass of water. This again indicates that the initial loss of water for this product ion was by way of the five-membered ring formation shown in Scheme **2**. This second loss of water in the fourth stage of mass spectrometry results from the dehydration of the intact C-terminal amide or another five-membered ring at the N-terminus. The fragmentation of the $[w_3' + H - H_2O]^+$, shown in Figure 2d, results in a mass loss of 151.03 Da, $B_3(C)_{II}$, with the resulting product ion designated as $[w_3' + H - H_2O - B_3(C)_{II}]^+$.

Tandem-mass spectrometry of the 4-mer PNA AACT $[M + H]^+$ ion with an acetylated N-terminus. We have argued that the N-terminus is involved in the protonation of PNAs and subsequently many of the fragmentation mechanisms. The results of the computational investigation, showing the potential intermolecular interactions and PA of the N-terminus, compared to the experimental data, involving very little sequence information, would suggest that proton sequestering at the N-terminus is occurring. In an effort to learn more about the role that the N-terminus plays in fragmentation, removal of this most basic site is essential. Acetylation replaces the basic primary amine with an acetyl group making the PNA backbone homogenous. Molecular mechanics and semiempirical calculations show that for a potential minimal energy conformation of acetylated-AACT the proton affinity of the first amine is about 26 kcal/mol less than the AACT terminal amine. This modification will clearly eliminate proton sequestering by the N-terminus of PNAs and grant more proton mobility.

It has already been mentioned that the only MS^2 product ion of the singly charged 4-mer PNA is the loss of water; however, CID of the acetylated PNA, Figure 4, results in primarily two product ions, the loss of the

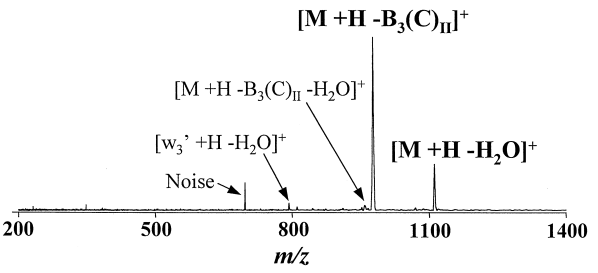

Figure 4. CID of the N-acetylated PNA results in two product ions, the loss of water, $[M + H - H_2O]^+$, and the loss of the cytosine attached to its methylene carbonyl linker, $[M + H - B_3(C)_{II}]^+$. Ion isolation of m/z = 1127.4; SORI-CID applied at m/z = 1145.5 (1000 Hz off-resonance) with an amplitude of 6.0 $V_{P\text{-}P}$ resulting in a KE_{lab} = 4.1 eV.

cytosine attached to its methylene carbonyl linker, $[M + H - B_3(C)_{II}]^+$, and the loss of water, $[M + H - H_2O]^+$. Two low intensity product ions also appear due to dissociation of the $[M + H - B_3(C)_{II}]^+$ and/or $[M + H - H_2O]^+$ peaks. The dominant decomposition pathway at the SORI amplitude used for the dissociation of AACT, 6.0 $V_{p\text{-}p}$ resulting in a KE_{lab} of 4.1 eV, is the loss of the cytosine attached to the methylene carbonyl linker with a ratio of 3.5:1, $[M + H - B_3(C)_{II}]^+$:$[M + H - H_2O]^+$.

The presence of the two major product ions resulting from the CID of the modified PNA supports the mobile proton theory [31–37]. The basic primary amine on the unmodified PNA appears to sequester the proton around the N-terminus due to high proton affinity and intramolecular interactions. Therefore, the dominant decomposition pathway is loss is water by the nitrile formation at the C-terminus, which is charge remote, or by the five-membered ring formation at the N-terminus, which depends on the location of the charging proton. However, when the basic primary amine is replaced by a homogenous backbone (N-acetylation) the increased proton mobility lowers the activation of the loss of the methylene carbonyl linker containing a cytosine, $[M + H - B_3(C)_{II}]^+$, enough to make it the dominant fragment in the MS^2. This is not surprising because, as discussed before, tertiary amides are more basic than the primary and secondary amides [91]. The loss of cytosine attached to the methylene carbonyl linker, Scheme **5**, is the only product ion observed where the fragmentation mechanism involves protonation on a tertiary amide. Almost all other fragmentations observed for the unmodified 4-mer PNAs involves neighboring group participation from the protonated primary amine on the N-terminus [87].

As stated before, it is known that the decomposition of peptides generally requires the presence of the proton [31–37]. This cleavage, loss of $B_3(C)_{II}$, is far from the N-terminus, Figure 1, and suggests that the homogeneity introduced by the acetylation allows the charging proton to move more freely about the PNA structure. This increases the chances that the proton could reside at the tertiary amide connecting the methylene carbonyl

linker attached to the cytosine subsequently allowing this fragmentation.

Conclusion

Clearly, CID of monoprotonated PNA oligomers does not provide sufficient information for their structural elucidation or characterization. More information will need to be obtained for the fragmentation pathways of gas-phase PNAs; however, from this experimental and theoretical investigation of PNAs we now know that the N-terminus is involved in the initial protonation and many of the fragmentation mechanisms of PNAs. These studies have also revealed that the primary amine of the unmodified PNA is responsible for proton sequestering at the N-terminus. We have also determined that water loss occurs at the C-terminal primary amide (preferred) and at the PNA N-terminus for the unmodified PNAs. A complete knowledge of PNA fragmentation in terms of trends, nucleobase effects, and the effect of structural modifications will be essential in order to achieve complete structural elucidation of these highly stable oligonucleotide analogs. PNAs have the potential to be used medically as antisense and antigene therapeutics and as molecular biology tools; therefore, the development of methods to determine the primary structure and degradation products of specific sequences will prove invaluable. These studies also have the capacity to provide new insights regarding the fragmentation pathways of structurally similar DNA mimetics, peptides, and oligonucleotides.

Acknowledgments

The authors would like to express our appreciation of the financial support generously provided by the Merck Genome Research Institute (Grant #31), the Jeffress Memorial Trust (Grant #J-433), and the Department of Chemistry, Virginia Commonwealth University.

References

1. Uhlmann, E.; Peyman, A.; Will, D. W. *Encyclopedia of Cancer*; Academic: New York, 1997; Vol. X, pp 64–81.
2. Luo, J.; Bruice, T. C. *J. Am. Chem. Soc.* **1998,** *120*, 1115–1123.
3. Nielsen, P. E.; Egholm, M.; Berg, R. H.; Buchardt, O. *Science* **1991,** *254*, 1497–1500.
4. Egholm, M.; Buchardt, O.; Nielsen, P. E.; Berg, R. H. *J. Am. Chem. Soc.* **1992,** *114*, 1895–1897.
5. Egholm, M.; Nielsen, P. E.; Buchardt, O.; Berg, R. H. *J. Am. Chem. Soc.* **1992,** *114*, 9677–9678.
6. Egholm, M.; Behrens, C.; Christensen, L.; Berg, R. H.; Nielsen, P. E.; Buchardt, O. *J. Chem. Soc. Chem. Commun.* **1993**, 800–801.
7. Nielsen, P. E.; Egholm, M.; Berg, R. H.; Buchardt, O. *Science* **1991,** *254*, 1497–1500.
8. Hyrup, B.; Nielsen, P. E. *Bioorg. Med. Chem.* **1996,** *4*, 5–23.
9. Orum, H.; Nielsen, P. E.; Egholm, M.; Berg, R. H.; Buchardt, O.; Stanley, C. *Nucl. Acids Res.* **1993,** *21*, 5332–5336.
10. Wang, J.; Palecek, E.; Nielsen, P. E.; Rivas, G.; Cai, X.; Shiraishi, H.; Dontha, N.; Luo, D.; Farias, P. A. M. *J. Am. Chem. Soc.* **1996,** *118*, 7667–7670.
11. Betts, L.; Josey, J. A.; Veal, J. M.; Jordan, S. R. *Science* **1995,** *270*, 1838–1841.
12. Demidov, V.; Potaman, V. N.; Frank-Kamenetskii, M. D.; Egholm, M.; Buchardt, O.; Sonnichsen, S. H.; Nielsen, P. E. *Biochem. Pharmacol.* **1994,** *48*, 1310–1313.
13. Christensen, L.; Fitzpatrick, R.; Gildea, B.; Petersen, K. H.; Hansen, H. F.; Coch, T.; Egholm, M.; Buchardt, O.; Nielsen, P. E.; Coull, J.; Berg, R. H. *J. Peptide Sci.* **1995,** *3*, 175–183.
14. Almarsson, O.; Bruice, T. C.; Kerr, J.; Zuckerman, R. N. *Proc. Natl. Acad. Sci. USA* **1993,** *90*, 7518–7522.
15. Almarsson, O.; Bruice, T. C. *Proc. Natl. Acad. Sci. USA* **1993,** *90*, 9542–9546.
16. Torres, R. A.; Bruice, T. C. *Proc. Natl. Acad. Sci. USA* **1996,** *93*, 649–653.
17. Fenn, J. B.; Mann, M.; Meng, C. K.; Wong, S. F.; Whitehouse, C. M. *Science* **1989,** *246*, 64–71.
18. Smith, R. D.; Loo, J. A.; Edmonds, C. G.; Barinaga, C. J.; Udseth, H. R. *Anal. Chem.* **1990,** *62*, 882–899.
19. Covey, T. R.; Bonner, R. F.; Shushan, B. I.; Henion, J. *Rapid Commun. Mass Spectrom.* **1988,** *2*, 249–256.
20. McLuckey, S. A.; Vanberkel, G. J.; Glish, G. L. *J. Am. Soc. Mass Spectrom.* **1992,** *3*, 60–70.
21. McLuckey, S. A.; Habibigoudarzi, S. *J. Am. Chem. Soc.* **1993,** *115*, 12085–12095.
22. Biemann, K. *Protein Sci.* **1995,** *4*, 1920–1927.
23. Biemann, K. *Biomed. Environ. Mass Spectrom.* **1988,** *16*, 99–111.
24. Little, D. P.; Chorush, R. A.; Speir, J. P.; Senko, M. W.; Kelleher, N. L.; McLafferty, F. W. *J. Am. Chem. Soc.* **1994,** *116*, 4893–4897.
25. Loo, J. A.; Edmonds, C. G.; Smith, R. D. *Anal. Chem.* **1991,** *63*, 2488–2499.
26. Speir, J. P.; Senko, M. W.; Little, D. P.; Loo, J. A.; McLafferty, F. W. *J. Mass Spectrom.* **1995,** *30*, 39–42.
27. Butler, J. M.; Jiangbaucom, P.; Huang, M.; Belgrader, P.; Girard, J. *Anal. Chem.* **1996,** *68*, 3283–3287.
28. Griffith, M. C.; Risen, L. M.; Greig, M. J.; Lesnik, E. A.; Sprankle, K. G.; Griffey, R. H.; Kiely, J. S.; Freier, S. M. *J. Am. Chem. Soc.* **1995,** *117*, 831–832.
29. Takao, T.; Fukuda, H.; Coull, J.; Shimonishi, Y. *Rapid Commun. Mass Spectrom.* **1994,** *8*, 925–928.
30. Flora, J. W.; Muddiman, D. C. *Rapid Commun. Mass Spectrom.* **1998,** *12*, 759–762.
31. Rodgers, M. T.; Campbell, S.; Marzluff, E. M.; Beauchamp, J. L. *Int. J. Mass Spectrom. Ion Processes* **1995,** *148*, 1–23.
32. Somogyi, A.; Wysocki, V. H.; Mayer, I. *J. Am. Soc. Mass Spectrom.* **1994,** *5*, 704–717.
33. Ballard, K. D.; Gaskell, S. J. *Int. J. Mass Spectrom. Ion Processes* **1991,** *111*, 173–189.
34. Tang, X. J.; Thibault, P.; Boyd, R. K. *Anal. Chem.* **1993,** *65*, 2824–2834.
35. Fabris, D.; Kelly, M.; Murphy, C.; Wu, Z. C.; Fenselau, C. *J. Am. Soc. Mass Spectrom.* **1993,** *4*, 652–661.
36. Jones, J. L.; Dongre, A. R.; Somogyi, A.; Wysocki, V. H. *J. Am. Chem. Soc.* **1994,** *116*, 8368–8369.
37. Hunt, D. F.; Yates J. R. III; Shabanowitz, J.; Winston, S.; Hauer, C. R. *Proc. Natl. Acad. Sci. USA* **1986,** *83*, 6233–6237.
38. Wu, J.; Lebrilla, C. B. *J. Am. Soc. Mass Spectrom.* **1995,** *6*, 91–101.
39. Zhang, K.; Zimmerman, D. M.; Chung-Phillips, A.; Cassady, C. J. *J. Am. Chem. Soc.* **1993,** *115*, 10812–10822.
40. Dewar, M. J. S.; Dieter, K. M. *J. Am. Chem. Soc.* **1986,** *108*, 8075–8086.
41. Bliznyuk, A. A.; Schaefer, H. F. I.; Amster, I. J. *J. Am. Chem. Soc.* **1993,** *115*, 5149–5154.
42. Reyzer, M. L.; Brodbelt, J. S. *J. Am. Soc. Mass Spectrom.* **1998,** *9*, 1043–1048.
43. Locke, M. J.; Hunter, R. L.; McIver, R. T. J. *J. Am. Chem. Soc.* **1979,** *101*, 272–273.

44. Isa, K.; Omote, T.; Amaya, M. *Org. Mass Spectrom.* **1990,** *25*, 620–628.
45. Kinser, R. D.; Ridge, D. P.; Uggerud, E. *Proceedings from the 39th Conference on Mass Spectrometry and Allied Topics;* Nashville, TN, May 19–24 1991.
46. Bojesen, G. J. *J. Am. Chem. Soc.* **1987,** *109*, 5557–5558.
47. Gorman, G. S.; Speir, J. P.; Turner, C. A.; Amster, I. J. *J. Am. Chem. Soc.* **1992,** *114*, 3986–3988.
48. Bojesen, G. J. *J. Chem. Soc. Chem. Commun.* **1986**, 244–245.
49. Lias, S. G.; Liebman, J. F.; Levin, R. D. *J. Phys. Chem. Ref. Data* **1984,** *13*, 695–808.
50. Gauthier, J. W.; Trautman, T. R.; Jacobson, D. B. *Anal. Chim. Acta* **1991,** *246*, 211–225.
51. Loo, J. A.; Udseth, H. R.; Smith, R. D. *Rapid Commun. Mass Spectrom.* **1988,** *2*, 207–210.
52. Katta, V.; Chowdhury, S. K.; Chait, B. T. *Anal. Chem.* **1991,** *63*, 174.
53. Meng, C.-K.; McEwen, C. N.; Larsen, B. S. *Rapid Commun. Mass Spectrom.* **1990,** *4*, 151–155.
54. Thomson, S. A.; Josey, J. A.; Cadilla, R.; Gaul, M. D.; Hassman, C. F.; Luzzio, M. J.; Pipe, A. J.; Reed, K. L.; Ricca, D. J.; Wiethe, R. W.; Nobel, S. A. *Tetrahedron* **1995,** *51*, 6179–6194.
55. Hannis, J. C.; Muddiman, D. C. *Rapid Commun. Mass Spectrom.* **1998,** *12*, 443–448.
56. Wahl, J. H.; Hofstadler, S. A.; Smith, R. D. *Anal. Chem.* **1995,** *67*, 462–465.
57. Marshall, A. G.; Hendrickson, C. L.; Jackson, G. S. *Mass Spectrom. Rev.* **1998,** *17*, 1–35.
58. Allinger, N. L. *J. Am. Chem. Soc.* **1977,** *99*, 8127–8134.
59. Dewar, M. J. S.; Zoebisch, E. G.; Healy, E. F.; Stewart, J. J. P. *J. Am. Chem. Soc.* **1985,** *107*, 3902–3909.
60. Wu, J. Y.; Lebrilla, C. B. *J. Am. Chem. Soc.* **1993,** *115*, 3270–3275.
61. Schmidt, M. W.; Baldridge, K. K.; Boatz, J. A.; Elbert, S. T.; Gordon, M. S.; Jensen, J. H.; Koseki, S.; Matsunaga, N.; Nguyen, K. A.; Su, S. J.; Windus, T. L.; Dupuis, M.; Montgomery, J. A. *J. Comput. Chem.* **1993,** *14*, 1347–1363.
62. Hehre, W. J.; Stewart, R. F.; Pople, J. A. *J. Chem. Phys.* **1969,** *51*, 2657–2664.
63. Hehre, W. J.; Ditchfield, R.; Stewart, R. F.; Pople, J. A. *J. Chem. Phys.* **1970,** *52*, 2769–2773.
64. Alexander, A. J.; Thibault, P.; Boyd, R. K. *Rapid Commun. Mass Spectrom.* **1989,** *3*, 30.
65. Tang, X.-J.; Boyd, R. K. *Rapid Commun. Mass Spectrom.* **1992,** *6*, 651.
66. Thorne, G. C.; Ballard, K. D.; Gaskell, S. J. *J. Am. Soc. Mass Spectrom.* **1990,** *1*, 249.
67. Burlet, O.; Yang, C.-Y.; Gaskell, S. J. *J. Am. Soc. Mass Spectrom.* **1992,** *3*, 337.
68. Cox, K. A.; Gaskell, S. J.; Morris, M.; Whiting, A. *J. Am. Soc. Mass Spectrom.* **1996,** *7*, 522–531.
69. Aue, D. H.; Bowers, M. T. In *Gas-Phase Ion Chemistry*; Bowers, M. T., Ed.; Academic: New York, 1979; Vol. 2, pp 1–51.
70. Wu, Z.; Fenselau, C. *J. Am. Soc. Mass Spectrom.* **1992,** *3*, 863–866.
71. Li, X. P.; Harrison, A. G. *Org. Mass Spectrom.* **1993,** *28*, 366–371.
72. Nair, H.; Wysocki, V. H. *Int. J. Mass Spectrom. Ion Processes* **1998,** *174*, 95–100.
73. Bouchonnet, S.; Hoppilliard, Y. *Org. Mass Spectrom.* **1992,** *27*, 71–76.
74. Jensen, F. *J. Am. Chem. Soc.* **1992,** *114*, 9533–9537.
75. Locke, M. J.; McIver, R. T. *J. Am. Chem. Soc.* **1983,** *105*, 4226–4232.
76. Green-Church, K. B.; Limbach, P. A. *J. Am. Soc. Mass Spectrom.* **2000,** *11*, 24–32.
77. Hunter, E. P.; Lias, S. G. *J. Phys. Chem. Ref. Data* **1998**, *27*, 413–656.
78. Green, M. K.; Lebrilla, C. B. *Mass Spectrom. Rev.* **1997,** *16*, 53–71.
79. Roepstorff, P.; Fohlman, J. *Biomed. Mass Spectrom.* **1984,** *11*, 601–602.
80. Reid, G. E.; Simpson, R. J.; O'Hair, R. A. J. *J. Am Soc. Mass Spectrom.* **1998,** *9*, 945–956.
81. Uhlmann, E.; Peyman, A.; Breipohl, G.; Will, D. W. *Angew. Chem. Int. Ed.* **1998,** *37*, 2796–2823.
82. Ballistreri, A.; Garozzo, D.; Maravigna, P.; Montaudo, G.; Giuffrida, M. *J. Poly. Sci.: Part A: Polym. Chem.* **1987,** *25*, 1049–1063 and references within.
83. Lin, H.-Y.; Ridge, D. P.; Uggerud, E.; Vulpius, T. *J. Am. Chem. Soc.* **1994,** *116*, 2996–3004.
84. Nold, M. J.; Cerda, B. A.; Wesdemiotis, C. *J. Am. Soc. Mass Spectrom.* **1999,** *10*, 1–8.
85. Dongre, A. R.; Jones, J. L.; Somogyi, A.; Wysocki, V. H. *J. Am. Chem. Soc.* **1996,** *118*, 8365–8374.
86. Eriksson, M.; Christensen, L.; Schmidt, J.; Haaima, G.; Orgel, L.; Nielsen, P. E. *New J. Chem.* **1998**, 1055–1059 and references within.
87. Tu, Y.-P.; Harrison, A. G. *J. Am. Soc. Mass Spectrom.* **1998,** *9*, 454–462.
88. McCormack, A. L.; Somogyi, A.; Dongre, A. R.; Wysocki, V. H. *Anal. Chem.* **1993,** *65*, 2859–2872.
89. Seela, F.; Roling, A. *Nucl. Acids Res.* **1992,** *20*, 55–61.
90. Shampine, L. J.; Ding, J.; Davis, R. G.; Anderegg, R. J. *Proceedings from the 42nd Conference on Mass Spectrometry and Allied Topics*; Chicago, IL, 1994; pp 114–115.
91. Witt, M.; Grutzmacher, H.-F. *Int. J. Mass Spectrom. Ion Processes* **1997,** *165*, 49–62.